Detection and resolution of drifting gratings by motion detectors in the fish retina

Vadim Maximov*, Elena Maximova, Ilija Damjanović and Paul Maximov

Institute for Information Transmission Problems
Russian Academy of Sciences
Bolshoi Karetny per., 19
Moscow 127994 GSP-4, Russia
*maximov@iitp.ru

Fish have highly developed vision that plays an important role in detecting and recognizing objects in different forms of visually guided behavior. All of these behaviors require high spatial resolution. The theoretical limit of spatial resolution is determined by the optics of the eye and the density of photoreceptors. However, further in the fish retina, each bipolar cell may collect signals from tens of photoreceptors, and each ganglion cell may collect signals from tens to hundreds of bipolar cells. If we assume that the input signals in this physiological funnel are simply summed, then fine gratings that are still distinguishable at the level of cones should not differ from the homogeneous surface for the ganglion cells. It is therefore generally considered that the resolution of the eye is determined not by the density of cones, but by the density of ganglion cells. Given the size of the receptive field of ganglion cells, one can conclude that the resolving power at the output of the fish retina should be ten times worse than at its input. But this contradicts the results of behavioral studies, for, as it is known, fish are able to distinguish periodic gratings at the limit of resolution of the cones. Our electrophysiological studies with extracellular recording of responses of individual ganglion cells to the motion of contrast gratings of different periods showed that the acuity of ganglion cells themselves is much higher and is close to the limit determined by the density of cones. The contradiction is explained by the fact that ganglion cells are not linear integrators of the input signals, their receptive fields being composed of subunits with significantly smaller zones of signal summation where nonlinear retinal processing takes place.

Keywords: Goldfish; spatial resolution; retina; ganglion cells; tectum opticum; direction selectivity; orientation selectivity.

1. Introduction

With few exceptions, fish inhabit a visually rich environment. Accordingly, they possess highly developed vision, which plays an important role in different forms of visually guided behavior: in object detection and recognition, in orientation and navigation, in foraging and avoiding predators, in habitat selection in sedentary species, in social behavior, including the territorial or schooling behaviors and the

---

*Corresponding author.

formation of mating pairs, in optical signaling for intraspecific and interspecific communication, etc. All of these behaviors require good visual acuity to detect, recognize and resolve ecologically relevant objects.

Visual acuity has been extensively investigated in many fish species using various methods starting from determination of the minimum angular size of prey to which the fish react from some distance (Hairston *et al.*, 1982; Li *et al.*, 1985; Browman *et al.*, 1990; Miller *et al.*, 1993; Mussi *et al.*, 2005), determination of the minimum grating period in the optomotor drum to which the fish display optokinetic or optomotor responses (Neave, 1984; Schaerer & Neumeyer, 1996; Dobberfuhl *et al.*, 2005; Haug *et al.*, 2010), to the measurements of minimum detectable grating period using classical conditioning, or different training method with food reward upon presentation of a grating pattern against a uniform field (Northmore & Dvorak, 1979; Bilotta & Powers, 1991; Neumeyer, 2003; Northmore *et al.*, 2007) or one grating of certain orientation against the second grating of the orientation orthogonal to the first one (Nakamura, 1968). Nevertheless, the span of definitions for behavioral visual acuity and the variety of methods to measure it allowed to obtain concordant findings. In particular, in case of the goldfish the spatial resolution, defined as the spatial frequency of minimally distinguishable grating, was about two cycles per degree, and thus, the visual acuity, defined as the half-period of this grating, was about a quarter of a degree (Hodos & Yolen, 1976; Northmore & Dvorak, 1979; Bilotta & Powers, 1991; Neumeyer, 2003).

The theoretical limit of spatial resolution is determined by the optics of the eye and the density of photoreceptors. Indeed, as is known from comparisons of the behavioral and histological studies, fish are more or less able to distinguish periodic gratings near this limit (Northmore & Dvorak, 1979; Browman *et al.*, 1990; Miller *et al.*, 1993; Northmore *et al.*, 2007; Haug *et al.*, 2010). However, further in the fish retina, each bipolar cell may collect signals from tens of photoreceptors, and each ganglion cell (GC) may collect signals from tens to hundreds of bipolar cells. If we assume that the input signals in this physiological funnel are simply summed, then fine gratings still distinguishable at the level of cones should not differ from the homogeneous surface for the GCs. It is therefore generally considered that the resolution is determined not by the density of cones, but by the size of the GC receptive field (RF) (Enroth-Cugell & Robson, 1966; Peichl & Wässle, 1979; DeVries & Baylor, 1997; Lee & Stevens, 2007). The retinal GCs can be of various types, project into various parts of the brain and perform different functions in different forms of behavior. As the visual field is covered by many GC mosaics, different sizes of the RFs of these mosaics may impose different restrictions on the visual function they serve. In fish, retinal GCs project to about a dozen distinct brain centers (Sharma, 1972; Northcutt & Wullimann, 1988; Burrill & Easter, 1994; Deguchi *et al.*, 2005), but it seems that only tectum opticum is responsible for behaviors that require high resolution.

The tectum opticum is the principal visual center that plays a crucial role in the information processing and control of visual behavior in the fish. Many aspects

related to the properties of the GCs terminating in the fish tectum opticum have been well established through decades of research — starting from the pioneering works by Jacobson & Gaze (1964) and Cronly-Dillon (1964). Up to a dozen types of retinal GCs that detect perceptually significant features form an ordered retinotopic projection in the fish tectum opticum. Their axons terminate at different depths in the tectum, what is reflected in ordered sequences of responses recorded in single-unit electrophysiological studies (Jacobson & Gaze, 1964; Zenkin & Pigarev, 1969; Maximova *et al.*, 1971). Those units that are recorded in the most superficial layers of the visually responsive zone have the property of the directional selectivity. These detectors respond to the stimuli moving in a particular (prefered) direction and give no response to the stimuli moving in the opposite or null direction. On the grounds that the application of a synaptic transmission blocker to the tectal surface does not eliminate responses of these units, it was concluded that these responses originate from the terminals of optic nerve fibers (Maximova *et al.*, 2012). And on the grounds that the intraocular injection of drugs, usually affecting the directional selectivity, eliminates optomotor response, it was concluded that the optomotor response is determined by the direction-selective (DS) GCs (Mora-Ferrer *et al.*, 2005). It was shown that in *Carassius gibelio*, the wild form of the goldfish, DS GCs are divided into three distinct groups prefering either caudo-rostral, ventro-dorsal, or dorso-ventral directions that separated by about 120° (Maximov *et al.*, 2005a,b). Each group, in turn, is represented by the ON and OFF cell subtypes in relatively equal amount, thus giving in total six subtypes of DS GCs. Recently, the existence of three groups of prefered directions in the direction-selective retinal inputs to the tectum was confirmed for larval zebrafish, *Danio rerio* with the use of a completely different experimental method (Gabriel *et al.*, 2012; Nikolaou *et al.*, 2012). Orientation-selective (OS) units of two subtypes or detectors of horizontal and vertical lines (Maximova & Maximov, 1981; Maximova, 1999; Maximov *et al.*, 2009) are excited by edges, stripes or gratings of one of the two orientations close to vertical or horizontal, both stationary and moving, regardless of the sign of contrast. Their recording sites were deeper than those of DS units. The existence of two subtypes of orientation-selective ganglion cells projecting to the tectum were also confirmed for larval zebrafish (Nikolaou *et al.*, 2012).

Of all detectors projecting to the fish tectum, DS and OS GCs have the smallest RFs. Widths of responsive parts of their RFs were estimated by various methods in our previous works (Damjanović *et al.*, 2009a,b) with the use of moving edges and stationary flashing light and dark stripes or light and dark spots. It was shown that both cell types are characterized by responsive receptive fields (RRFs) with the mean width of the order of 4−5 angular degrees. For the fish of medium size, this corresponds to an area with diameter of about $300 \, \mu$m on the retina (Maximov *et al.*, 2005b), which is consistent with the average size of the dendritic tree of DS GCs (Maximova *et al.*, 2006). Even if we consider only the long-wavelength-sensitive cones (which mainly determine the responses of DS GCs), up to 360 of these cones fall into the RF of such diameter, indicating a high convergence of the cones onto the

GCs. Since it is unlikely that GCs projecting to other brain nuclei have smaller RFs, and since the goldfish retina is relatively homogeneous and lacks a specialized area of high cell density (Johns & Easter, 1977), one must recognize that the maximum spatial resolution is provided by the DS and/or OS GCs.

To resolve the discrepancy between high visual acuity observed in behavioral experiments, and large RFs of GCs (as well as their large dendritic fields) in the present study we investigate the spatial properties of GCs with the use of gratings of different spatial frequency. It turned out that the real GCs does not behave as simple linear integrators of the input signals with broad RFs, and the width of their RF does not determine the spatial resolution of the fish visual system, because in reality each GC is able to detect high-frequency gratings by itself.

2. Materials and Methods

2.1. *Experimental animals*

The experiments were performed with the cyprinid fish *Carassius gibelio* (Bloch, 1782), a closest wild relative of the goldfish. The fish were acquired from local suppliers (Moscow region), kept in aerated fresh water aquaria at room temperature and natural daylight regime for several months prior to experiments and fed with live food. The fish were treated in accordance with the European Communities Council Directive of 24 November, 1986. The experimental procedures were approved by the local ethical committee of the Institute for Information Transmission Problems.

2.2. *Preparation*

For the electrophysiological experiment a fish of $10-15$ cm standard body length with exposed optic tectum was immobilized with tubocurarine (0.3 mg per 100 g of body weight), placed in a Plexiglas tank and fixed in natural position with perfusion of aerated water through its gills. The water level in the tank was maintained so that the eyes of the fish were under water but the water was not poured into the brain. The fish looked on the monitor screen with its right eye through the transparent tank wall. Visual responses were recorded from a contralateral lobe of the tectum opticum. The surgical procedure was described in detail elsewhere (Damjanović *et al.*, 2009a).

2.3. *Visual stimulation*

Visual stimuli were presented to the fish on the computer-controlled 17 inch CRT monitor LG Flatron 775FT from the distance of about 30 cm. From this distance the screen occupied $43 \times 32°$ of the fish visual field. To stimulate the motion detectors, moving contrast edges or square-wave gratings were presented on the screen within a square area of stimulation with angular dimensions of $11 \times 11°$. When calculating the angular size of the stimuli the refraction of the rays on the front wall of the tank was taken into account. The stimulation area could be placed at arbitrary locations of the screen and was usually placed so that the RF of the recorded unit was located in its center.

Achromatic stimuli were dark or light and were presented on an intermediate gray background. Specific values of their luminances in the experiments did not matter, because in case of sufficient contrast the responses of motion detectors are essentially independent of the brightness of a moving stimulus and of background (Maximov *et al.*, 2005b, 2009). Nevertheless, most of the experiments were performed under similar lighting conditions. Usually, the luminance of the background was maintained at $8.5\,\mathrm{cd\,m^{-2}}$, when expressed in terms of photopic human vision. According to our data (Maximov *et al.*, 2007) the photopic spectral sensitivity of the fish movement detectors is determined mainly by its red-sensitive cones. So, it is natural to specify the brightness of the screen "from the point of view" of the red-sensitive cones. In these terms, the background usually has the effective radiance of $14.5\,\mathrm{mW\,m^{-2}\,sr^{-1}}$, and the effective radiances of the light and dark stimuli were respectively 65 and $0.13\,\mathrm{mW\,m^{-2}\,sr^{-1}}$. Constant brightness was maintained for the rest of the monitor screen outside the stimulation area, which effective radiance was usually equal to $7.0\,\mathrm{mW\,m^{-2}\,sr^{-1}}$.

2.4. *Data acquisition*

Single-unit responses of DS and OS GCs were recorded extracellularly from their axonal terminals in the superficial tectal retinorecipient layers, using low impedance $(200-500\,\mathrm{K\Omega})$ recording microelectrodes made from metal-filled micropipette and tipped with a platinum cap of $2-10\,\mu\mathrm{m}$ in diameter (Gestesland *et al.*, 1959). The microelectrode was guided to a necessary tectal area under visual control by means of a micromanipulator according to the retinotopic projection (Jacobson & Gaze, 1964). Neuronal discharges were amplified, filtered, displayed on an oscilloscope, fed to an audio monitor, digitized by an A/D converter (25 kHz sampling rate), and loaded into the computer. The units were isolated by adjusting the position of the microelectrode. Once a single unit recording was obtained (as can be judged by the absence of the interspike intervals that are shorter than the period of absolute refractoriness), the unit's responses to various stimuli were recorded, and the preferable stimulus was found. Responses, loaded into the computer during the registration interval, were stored in the database, either without preprocessing (for subsequent analysis of spike form), or after filtering according to the amplitude discrimination. In this case they were stored as a sequence of time points of the spike appearance for further analysis.

Visual stimulation and data acquisition were guided by independent computer modules. These modules were mutually connected and synchronized in the experimental setup with a third independent computer, which served for the on-line graphic demonstration of the processed results and for the operative control of stimulation and recording parameters during the experiment. The system of three mutually connected and synchronized computer modules used in the setup is described in detail elsewhere (Maximov *et al.*, 2005b; Damjanović *et al.*, 2009a).

2.5. *Procedure*

When a good DS or OS unit was isolated and an approximate position of its RF was found the first step was always to measure its directional tuning curve (polar diagram) with contrast edges moving in different directions across the RF. This allowed to confirm the type of the recorded unit and to determine the size and location of its RF. The next step was to measure the response function of the unit by gratings of different spatial frequency.

2.5.1. *Polar diagram measurements*

A typical procedure for the measurement of a polar diagram by moving contrast edges was as follows. The monitor and the stimulation area on its screen were placed in the visual field of the fish in such a way as to cover the estimated RF, and the values of the following stimulation parameters were specified: the speed of movement of the edge, the brightness of the background and of the edge, as well as the brightness of the sur- roundings outside the stimulation area, the initial direction of movement, the total number of different directions of movement (usually 12 or 24), and the number of repetitive runs in each direction. After that, measurement was performed automatically for different directions in a quasi-random order. At the end of the procedure, a mea- surement for the first direction was repeated in order to check the unit response level. The mean number of spikes, N, in the response (over several repeated runs in each direction) as a function of direction φ was approximated by a second order harmonic function:

$$N(\varphi) = a_0 + a_1 \cdot \cos(\varphi - \varphi_1) + a_2 \cdot \cos(2\varphi - 2\varphi_2).$$

The amplitudes of the zero (a_0), first (a_1) and second (a_2) harmonics, and the phases of the first (φ_1) and second (φ_2) harmonics characterize the directional tuning curve.

According to their polar diagrams GCs are subdivided into nonselective, direction- selective, and orientation-selective. The three types differ from each other by the relative contribution of different harmonics. The amplitudes of the first and second harmonics reflect the relative strength of the directional and orientational compo- nents, respectively, and thus, can be considered as classifying features. DS and OS units that fall into the domains, where $a_1 > \frac{1}{2} a_0$ and $a_1 > a_2$, or $a_2 > \frac{1}{2} a_0$ and $a_1 < a_2$, respectively, were the subject of the present study. The prefered directions and prefered orientations of the DS and OS GCs under study can be determined from the phases of the first and the second harmonics.

2.5.2. *Determination of the RRF center*

Position of the RRF in the stimulation area was calculated online using the same experimental data, obtained during polar diagram measurements. The RRF center was estimated from the sequences of time points of spike appearances in all of the trials for all directions of movement. The idea of an automatic procedure that determined the position of the RRF center is as follows. A squared deviation of the time of spike appearance from the time when the stimulus passes through the

assumed RRF center is calculated for each of the applied directions. The center of the RRF was determined as a point in the visual field, where the mean square deviation calculated for all directions was minimal. After the measurement of the polar diagram and determination of the position of the RRF, the position of the area of stimulation on the monitor screen was centered with respect to the RRF, and all subsequent procedures were conducted with the centered RRF.

2.5.3. *Measurement of responses to a set of grating stimuli*

Spike activity of motion detectors was recorded in response to the movement of square-wave gratings of various spatial frequencies into the RF and drifting them through it at a certain speed in a preferential direction. The other stimulation parameters (the speed of movement, brightness of the background and of the grating, as well as the brightness of the surroundings outside the stimulation area, and the number of repetitive runs of each grating) were specified in advance. In case of stable recordings the DS and OS units provide reproducible number of spikes in response to repeated stimulation. Therefore, the measurement was limited to three runs as a compromise between the desire to get more accurate numbers, and the desire to complete the entire measurement cycle before the cell is lost. The measurement began with the presentation of the moving edge. Then, a series of gratings of increasing spatial frequency was presented automatically. The finest grating used had a frequency of 1.8 cycles per degree. At the end of the procedure, a measurement for the moving edge was repeated.

3. Results

3.1. *Receptive field sizes of movement detectors*

The purpose of this section was to demonstrate on the basis of a large experimental data set that DS and OS GCs had quite large RFs that cannot provide good spatial resolution, given the assumption of linear signal processing within the RF. The structure of the GC RF was described in terms of the Gaussian model. According to this model, the magnitude of the cell response as a function of a stimulus position was approximated by a Gaussian curve. Parameters of the model were determined from post-stimulus histogram of spike discharge, evoked by adequately oriented contrast edge moving across the cell RF. This set of data was fitted by the Gaussian function with the use of a least-squares minimization algorithm. The equation for Gaussian curve is:

$$G(x) = \frac{N}{\sigma\sqrt{2\pi}} \exp\left(-\frac{(x - \bar{x})^2}{2\sigma^2}\right),$$

where x is the position of stimulus, $\bar{x}$ is the coordinate of approximated RRF center, σ is the standard deviation determining the Gaussian width and N is the total number of spikes in the discharge. The best Gaussian fit $G(x)$ was considered as an optimal approximation of the cell RRF.

For this study, we used the results of polar diagram measurements already stored in our database for several years. At first, for each diagram the prefered direction of

motion was determined. Then the nearest direction (of the whole set of directions used in measurement of the polar diagram) was found, and the corresponding discharge was approximated by a Gaussian curve. Figures 1(a), 1(b), 1(d) and 1(e) illustrate the procedure with examples of DS and OS GCs, and the histograms in Figs. 1(c) and 1(f) show the distributions of the RRF sizes for DS and OS GCs,
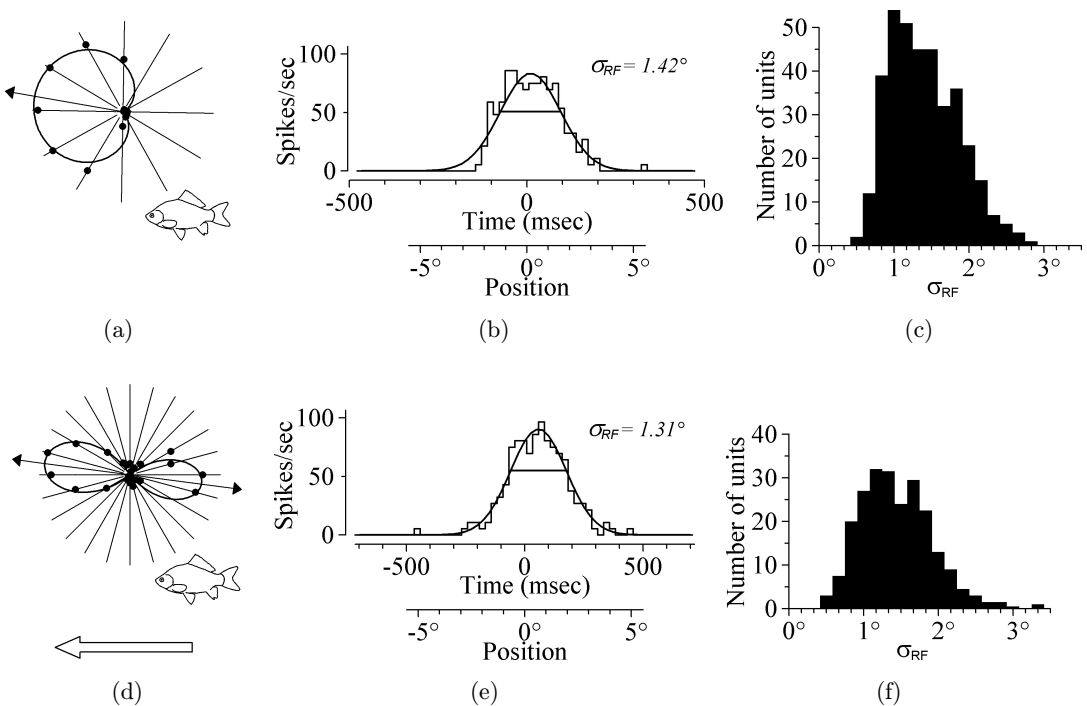

Fig. 1.   RRF sizes of DS and OS GCs determined from the duration of spike trains evoked by contrast edge moving in the preferred direction across the stimulation area. (a) An example of polar diagram of an OFF-type DS GC selective to caudo-rostral movement. Responses to dark edges moving in 12 directions at the speed of $16.5°$/s against a light background are presented in the diagram. Dots on rays of different direction mark the mean number of spikes evoked in response for each of the tested directions. Preferred direction of the cell is shown by a black arrow. An RRF size was estimated on the basis of the response, evoked by contrast edge moving in the direction closest to the preferred one, namely, a caudo-rostral direction shown by an open arrow at the bottom of Fig. 1. (b) Responses of the cell to stimulus moving in the caudo-rostral direction. Stepped solid curve is a post-stimulus histogram of the discharge, showing the number of evoked spikes along the time or position scales; the bell-shaped curve represents the best-fit Gaussian function. A horizontal chord of the Gaussian curve is drawn at the level of 0.607 of the maximum. The length of the chord at this level corresponds to twice the value of σ_{RF}, measured in units of visual angle. The time scale: zero point corresponds to the time when the stimulus leading edge passes through the center of stimulation area. The position scale: zero point corresponds to the position of center of stimulation area. The scale enables to fix the position of stimulus leading edge in the visual space in the moment of spike appearance. (c) Histogram of distribution of the RRF sizes for 371 DS GCs, expressed in terms of σ_{RF} -values of the best Gaussian fits, measured in units of visual angle. (d) An example of polar diagram of a detector of vertical line plotted on the basis of its responses to dark edges moving in 24 directions against gray background at the speed of $11°$/s. (e) Responses of the detector to stimulus moving in a caudo-rostral direction. Display format as in Fig. 1 (b). (f) Histogram of distribution of the RRF sizes for 231 OS GCs. Since for OS GCs there are two preferred directions (up and down for detectors of horizontal line, and back and forth for detectors of vertical line), separate approximations were built for that and for the other direction.

respectively. Both for the DS and for OS GCs the values of σ_{RF} lie between $0.5°$ and $3°$. For 371 DS GCs mean value of σ_{RF} is equal to $1.41 \pm 0.47°$, and for 231 OS GCs it is equal to $1.44 \pm 0.48°$.

In the frame of the simple linear model (see Appendix), the spatial resolution of the linear RF is uniquely determined by the value of σ_{RF}. When σ_{RF} takes the value of $1.4°$, typical for the motion detectors, the frequency characterizing the spatial resolution of such a linear system amounts only to a fraction of a cycle per degree (Fig. 11(c)), what is almost an order of magnitude worse than the resolution provided by the cone mosaic of the retina.

3.2. *Responses of movement detectors to grating stimuli*

A total of 73 DS GCs and 105 OS GCs were successfully isolated and investigated with drifting gratings. Each unit was studied with the full set of gratings moved with certain velocity in the prefered direction across the unit's RF. Results of the measurements were saved in a database as files of special format and processed off-line. In most cases, each unit was examined with sets of gratings of different brightness and moving at different speeds. In the case of the detectors of oriented lines, for which there are two preferred directions, the gratings may be moved in both directions. The numbers of examined GCs of each type as well as the total numbers of accumulated database records for them are shown in the Table 1.

An overall picture of the responses of the movement detectors to moving gratings did not depend either on the preferred direction or on the preferred orientation, but it only did on the selectivity to the sign of contrast. Thus, the results can be divided into three groups according to the type of units: ON, OFF and ON-OFF types. In case of the coarse square-wave gratings, DS GCs of the ON-type respond by burst discharges of activity to the leading edge of each light stripe (Fig. 2(a)) or to the trailing edge of each dark stripe crossing the RF. The discharge starts when the edge enters the RF and ends when it leaves the RF (therefore in Fig. 2 discharges begin noticeably before the upward deviations on the stimulus traces, which reflect changes in stimulus intensity in the center of the RF). Accordingly, the length of the discharge is determined by the width of the RF, and for the first discharge it is almost

Table 1. The numbers of examined GCs of each type and the amount of measurements made with moving gratings.

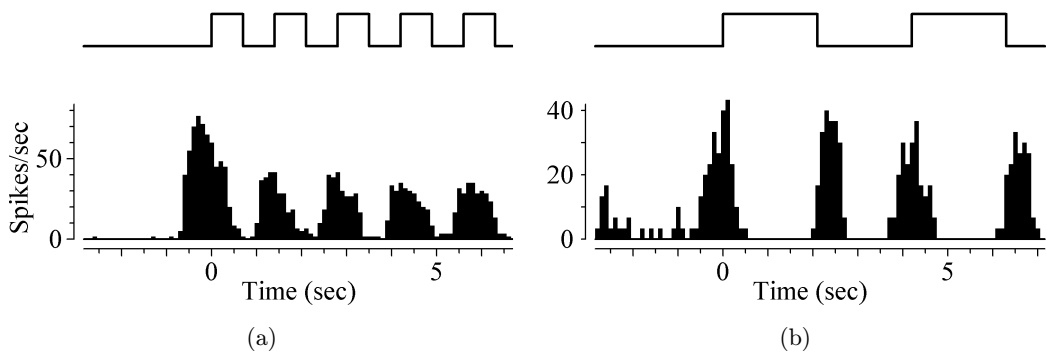| Type of Ganglion Cell	Number of Cells	Number of Measurements
ON-directional caudo-rostral	25	65
OFF-directional caudo-rostral	20	31
ON-directional ventro-dorsal	9	17
OFF-directional ventro-dorsal	7	11
ON-directional dorso-ventral	9	17
OFF-directional dorso-ventral	3	9
detector of horizontal line	65	162
detector of vertical line	40	99

Fig. 2. Typical post-stimulus histograms of motion detector's responses to drifting square-wave gratings. (a) Response of a direction-selective unit of the ON-type with a caudo-rostral preferred direction to movement of a light vertical square-wave grating with a spatial frequency of 0.26 cycles per degree. The motion was carried out at the speed of 2.75°/s in a caudo-rostral direction. (b) Response of a horizontal line detector to movement of a light horizontal square-wave grating with the spatial frequency of 0.09 cycles per degree. The motion was carried out at speed of 2.75°/s in a ventro-dorsal direction. Bin size, 100 ms. Origins on abscissas correspond to the moment when a leading edge of the gratings passes through the center of the stimulation area. Stimulus traces on top indicate stimulus intensity in the central point of the stimulation area during the motion of the grating. Lightening is given by upward deflection.

identical to the width determined from the polar diagram measurements for the same unit. When the spatial frequency of the grating increases, the magnitude of the bursts decreases, they begin to merge into a continuous discharge, and then at higher frequencies the density of the discharge decreases, and eventually it disappears altogether. Only the burst at the leading edge of the first stripe of the grating remains in the unit response. DS GCs of the OFF-type, in contrast, respond to the drifting gratings when the leading edge of each dark stripe or the trailing edge of each light stripe passes through the RF. In other respects their responses are indistinguishable from those of DS GCs of the ON-type.

Detectors of oriented lines are cells of the ON-OFF type. Therefore, they respond to movement of coarse square-wave gratings by bursts both to the leading and to the trailing edges of each stripe, which resulted in a doubling of the frequency of response — compare stimulus modulation and response modulation patterns in Fig. 2(b). The detector of horizontal line shown in Fig. 2(b), had a weak spontaneous activity in the dark (as it often happens with OS GCs), what explains the activity recorded before the leading edge of the light grating went into the RRF of the cell. Just as in the case of the DS units, with the increase of the spatial frequency of the grating the magnitude of the bursts decreases, responses to ON edges being reduced first. This decrease and the subsequent disappearance of the ON responses occurs fairly quickly, especially in the cells with large RFs. Even in cells with rather small RFs the ON responses disappear already at spatial frequencies of 0.25 cycles per degree. It should be noted that it is the responses of the ON-type that always disappear first, what is indicative of the differences in the mechanisms of generation of the ON and OFF responses. With the further increase of the grating frequency,

remaining OFF responses first begin to merge into a continuous discharge. Then the density of the discharge decreases and finally it disappears.

3.3. *Grating acuity of direction-selective ganglion cells*

The grating acuity can be determined (1) by the highest spatial frequency at which the grating can be discriminated from a uniform field, or (2) by the highest spatial frequency at which the system differentiates individual stripes of the grating. Generally speaking, this is not the same. In the case of motion detectors, which do not respond to sustained illumination, the discrimination of the grating from a uniform field means that the cell responds to a drifting grating with some sustained firing, while the discrimination of individual stripes requires reproduction of the fundamental frequency of the grating in the cell response. For definiteness, the first case will be called hereafter the detection of gratings, and the second one their resolution.

In order to analyze quantitatively the detection and resolution of gratings, the records of spike responses to drifting grating stimuli were Fourier analyzed to calculate the responses at DC and at the fundamental stimulus frequency. To do this, each record, corresponding to a particular frequency, was analyzed as follows. The first discharge of response to the movement of the leading edge of the grating through the RF was discarded. From the rest of the stimulation interval an integer number of periods of stimulation were selected, and the magnitudes of the zero and first harmonic components of the Fourier decomposition of the response were calculated for it. The dependences of the magnitude of the zero harmonic component of the Fourier decomposition of the response (which coincides with the mean spike rates of the response) and the spatial frequency dependence of the magnitude of the first harmonic component on the spatial frequency hereafter will be referred to as spatial frequency characteristics of the response. Examples of such characteristics are shown in Fig. 3. The figure also shows the theoretical spatial-frequency characteristics, calculated for linear models of RFs of the GCs. For this purpose the results of the presentation of a moving contrast edges (which were conducted along with the measurements by gratings) was used. The RF size was determined from the traces of the first and the last sessions of the experiment in the same way as it was determined from the results of measurement of a polar diagram (see Sec. 3.1). According to the obtained value of σ_{RF}, the theoretical curve was calculated (see Appendix).

As can be seen from the lines marked with circles in Fig. 3, both cells maintained a high level of the mean spike rate close to the maximum at high spatial frequencies, where the responses of the linear model were decreased by more than an order of magnitude. We can therefore conclude that in these cells visual acuity for detecting the presence of a grating was much higher than the acuity that was provided by linear RF of the appropriate size. Only at frequencies of the order of 1 cycle per degree the spike rate abruptly descended to the level of spontaneous activity, shown in the diagrams by the dashed horizontal lines (in DS GCs spontaneous activity was usually very low, of the order of several pulses per second). Such behavior of the mean spike
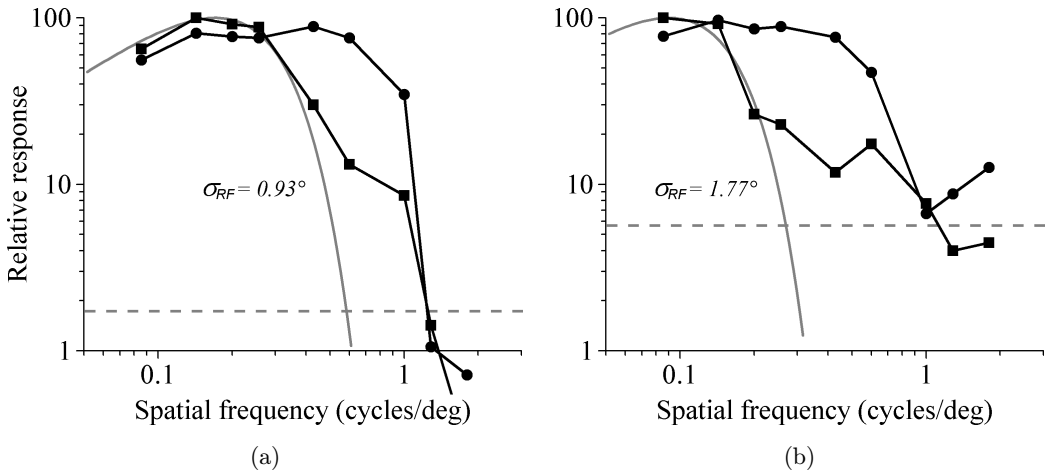
Fig. 3. Dependences of the mean spike rate (the zero harmonic) and of the amplitude of the fundamental frequency (the first harmonic) on the spatial frequency of the gratings for two DS GCs plotted in double logarithmic co-ordinates. (a) A unit of the OFF-type with small RF selective to dorso-ventral movement stimulated by horizontal black gratings drifting at the speed of 2.75°/s in a downward direction. (b) A unit of the OFF-type with large RF selective to caudo-rostral movement stimulated by vertical black gratings drifting at the speed of 2.75°/s in the caudo-rostral direction. Circle marks correspond to the mean spike rates of the units' response to stimulation with gratings of various spatial frequencies. Square marks represent the magnitude of the first harmonic component of the decomposition. Gray smooth curves represent theoretical predictions for response to the same stimuli of linear systems with corresponding sizes of the RF (see Appendix). Dashed horizontal lines indicate levels of spontaneous activity.

rate was characteristic for all the DS GCs investigated. The highest spatial frequency that produced a reliable response above the mean noise level should be considered as the definition of the physiological detection acuity of the GCs.

The curves for the first harmonic, shown by squares in Fig. 3, also fell off much slower at high frequencies than the theoretical curves. In other words, the real cells could reproduce such frequencies that the linear model could not. On the contrary, in the extreme low frequency range, the theoretical and experimental curves had the same behavior, and the low-frequency reproduction was entirely determined by the RF size of the GCs.

Reproduction of some frequency (presence of the first harmonic component in the cell response) automatically implies the existence of some nonzero spike rate at that frequency. It follows that the resolution acuity cannot be better than the detection acuity. At the same time, quite often we come across the GCs in which the resolution acuity is markedly below the detection acuity. An example of such cell is shown in Fig. 4, where in addition to the spatial frequency characteristics the post-stimulus time histograms of the cell responses to different drifting gratings are also shown. The histogram on the top represents the cell response to the movement of the black edge into the RF of the cell. According to the width of this discharge the RF width of the cell was determined. Below there are three poststimulus histograms of responses to the moving gratings of increasing frequency. Naturalistic images of
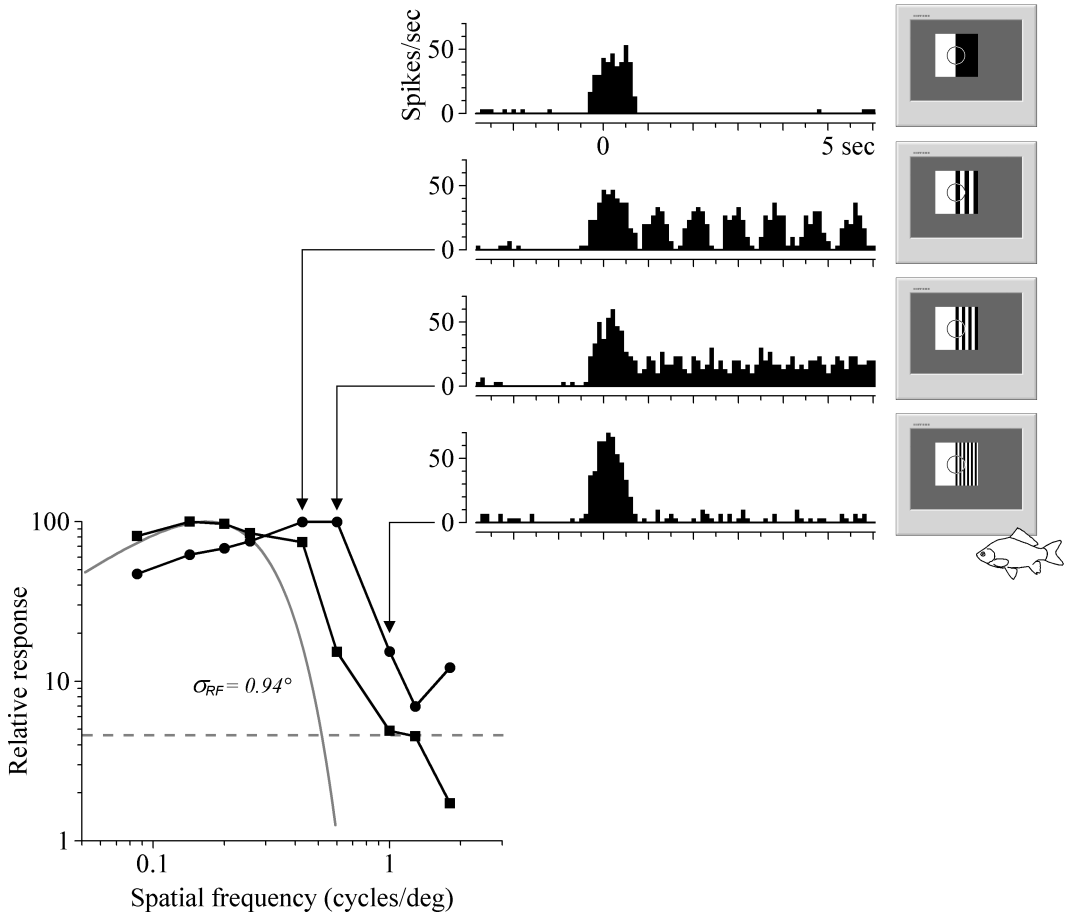
Fig. 4. Spatial frequency characteristics and temporal responses of a DS GC of the OFF-type with small RF selective to caudo-rostral movement stimulated by vertical black gratings of various spatial frequencies drifting at the speed of $2.75°$/s in the caudo-rostral direction. Other conventions are as in Figs. 2 and 3.

displays on the right are given to make it possible to compare the RF size of the cell and the grating periods. One can see that at first the cell responds by separate discharges at each stripe of the drifting grating. Then the discharges merge into a continuous discharge, the first harmonic component drops sharply in magnitude, while the magnitude of the zero component remains unchanged. At this point, the cell loses its ability to resolve stripes, but is still able to detect the grating at this spatial frequency. Finally, at the spatial frequency of 1 cycle per degree, the magnitude of the zero component also reduces. Only a burst to the leading edge of the grating remains.

All DS GCs recorded appeared to be quite diverse in the form of their spatial frequency characteristics and in the value of the spatial resolution. The highest spatial frequency of the grating, at which DS GCs responded, lay in the region of $1-2$ cycles per degree. These did not correlate with other properties of the cells, in particular, with the size of their RF. At the same time, changing of the stimulation parameters (such as
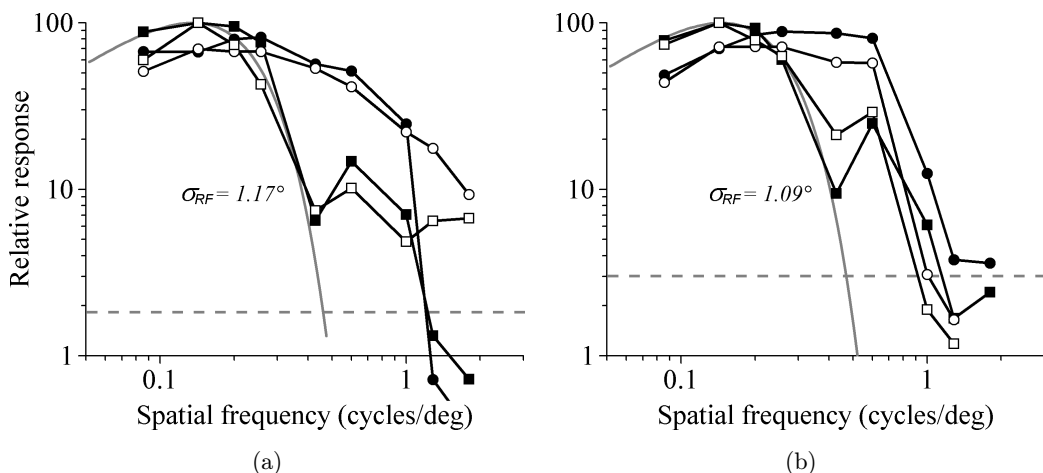
Fig. 5. Comparison of the spatial frequency charecteristics taken under different conditions of stimulation by drifting contrast gratings. (a) A DS GC of the ON-type selective to caudo-rostral movement stimulated by vertical black or white gratings drifting at the speed of $2.75°/s$ in the caudo-rostral direction. Black symbols show data for black gratings on the gray background (the mean effective radiance of the gratings was $7.4\,\mathrm{mW\,m^{-2}\,sr^{-1}}$, the Michelson contrast was 0.97), white symbols show data for white gratings on the same background (the mean effective radiance was $40\,\mathrm{mW\,m^{-2}\,sr^{-1}}$, the Michelson contrast was 0.64). In all cases, the effective radiance of the far surround equalled $7.0\,\mathrm{mW\,m^{-2}\,sr^{-1}}$. (b) A DS GC of the OFF-type selective to caudo-rostral movement stimulated by vertical black gratings drifting in the caudo-rostral direction with two different speeds. Black symbols show data for the speed of $2.75°/s$, white symbols shows data for the speed of $5.5°/s$. Other conventions are as in Fig. 3.

intensity or contrast of gratings or speed of movement) had little effect on the shape of the spectral curves. Figure 5(a) illustrates the results of two experiments in which sets of black and white gratings drifting on a gray background were presented to the same GC. Despite significant differences in the average brightness and contrast of gratings, the resulting spectral curves hardly differ from one another.

Movement of the periodic grating through the RF leads to a periodic stimulation of the cell's inputs over time. Therefore, one possible explanation for the drop of the spectral curves at high spatial frequencies could be that the cell behaves as a temporal low-pass filter and does not pass high-frequency flicker. If so, then the change in velocity of the gratings should have led to a shift of the spectral characteristics to the left. In particular, doubling of the speed must lead to a considerable shift of the position of the sharp drop of each curve. Figure 5(b) shows that this was not the case. In the experiments shown in Fig. 5, the absolute values of responses in different conditions of stimulation certainly were different, especially in the case of the gratings moving at different speeds. Therefore, for ease of comparison, the curves have been scaled to fit at the maxima of the first harmonics.

3.4. *Grating acuity of orientation-selective ganglion cells*

Most OS GCs tested with wide range of grating frequencies exhibited profound dependences of the zero and the first harmonic components on the stimulus
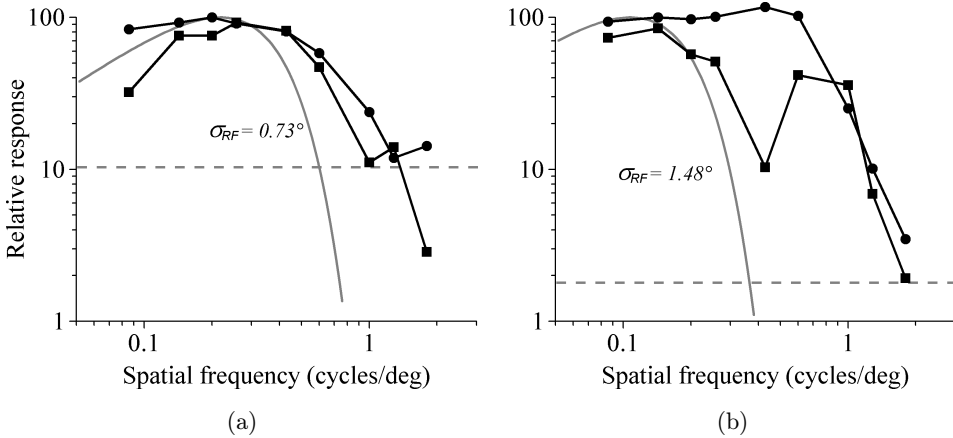
Fig. 6. Dependences of the zero and the first harmonic components on the spatial frequency of the gratings for two OS GCs. (a) A detector of horizontal line with small RF stimulated by horizontal white gratings drifting at the speed of 2.75°/s in the upward direction. (b) A detector of horizontal line with RF of medium size stimulated by horizontal black gratings drifting at the speed of 2.75°/s in an upward direction. Other conventions are as in Fig. 3.

frequency. As in the DS GCs, the patterns of this dependence were very diverse. Typical spatial frequency characteristics of the OS GCs are shown in Fig. 6. One can see that, in general, they look the same as the characteristics of the DS GCs. Cells have both the detection acuity and the resolution acuity well above the theoretical one. Meanwhile the presence of a cell response to drifting high-frequency gratings in the absence of the response to a uniform field does not mean that the cell responds to any high-frequency inhomogeneity. It has been shown that the OS GCs do not respond to high-frequency gratings perpendicular to the optimal one (for example, to presentation of a vertical grating to the detector of horizontal lines). Moreover, in this case, one can see a decrease of spontaneous activity, which confirms the existence of antagonistic relations between the orthogonal directions (Maximova & Maximov, 1981). This suggests that at high spatial frequencies OS GCs retain selectivity for orientation, which can serve as a basis for distinguishing between vertical and horizontal gratings in behavior. One noticeable difference from the DS GCs lies in the fact that in the low frequency range the OS GCs with small RF had small first harmonic component, what was quite understandable, since at low spatial frequencies, these cells displayed a frequency doubling — Fig. 6(a).

In contrast to the DS cells, some OS cells were found to have resolution even higher than 2 cycles per degree. For them, we failed to see the fall of resolution over the entire range of spatial frequencies tested. An example of such cell is shown in Fig. 7. That was a case of a stable single-unit recording for more than 3 hours, what made it possible to fully explore the properties of the cell. Repeated measurements of the width of the RF by different methods gave consistent results. The results of measurements by moving edges and flashing stripes are shown in Figs. 7(a) and 7(b). Approximation of the two histograms by Gaussian functions gave identical curves.
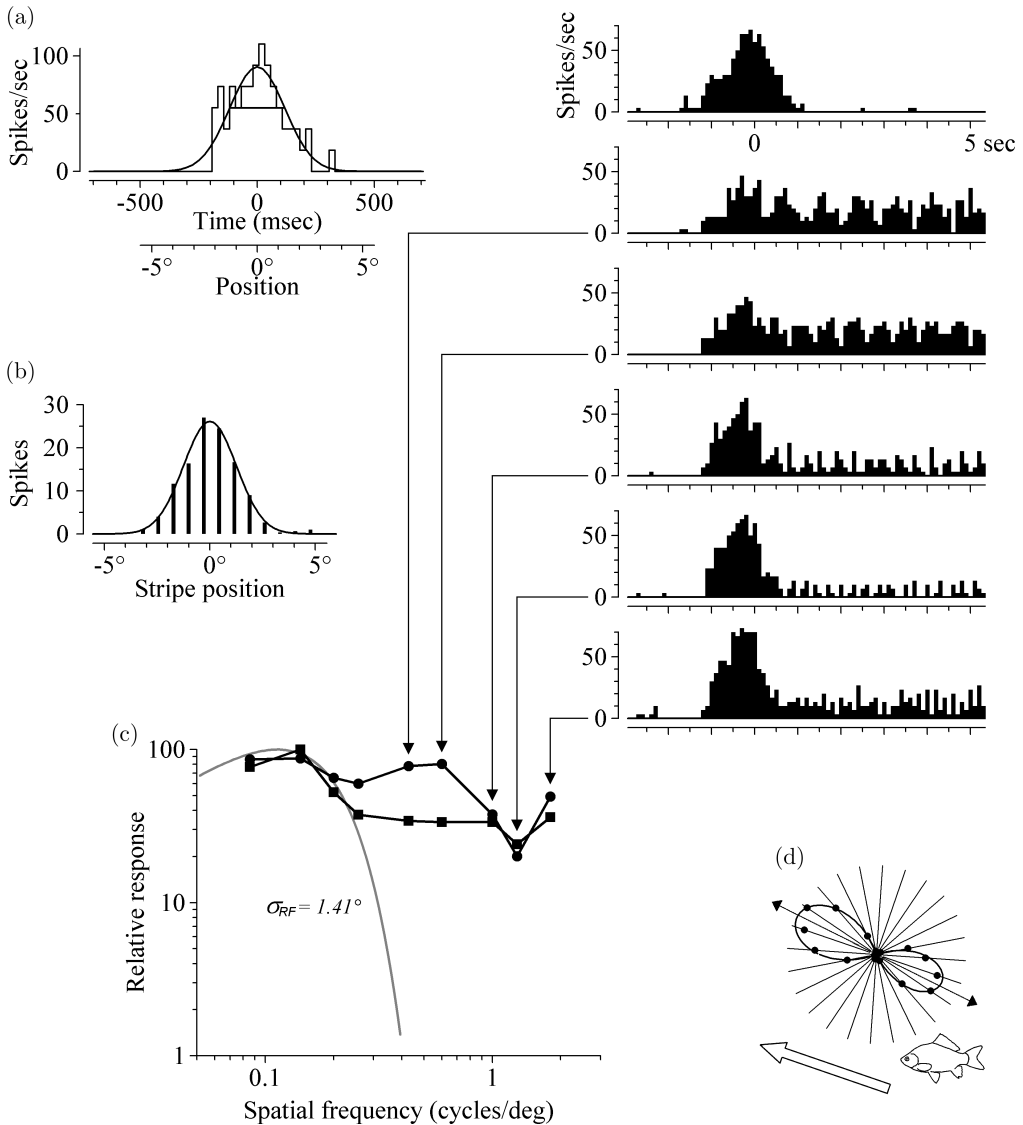
Fig. 7. The detector of vertical line possessing high spatial resolution. (a) RRF sizes of the unit determined from the spike trains evoked by black edge moving in the preferred direction across the stimulation area at the speed of 16.5°/s against a gray background. Conventions are as in Fig. 1(e). (b) Distribution of the unit responses to adequately oriented stationary black stripes of the width of 10 angular minutes flashing across the stimulation area. Stimuli flashed on and off sequentially at various places of the stimulation area in a quasi-random order. The number of spikes recorded during 500 ms after onset of the stimulus was a measure of the magnitude of the cell response. Widths of histogram bars correspond to the widths of stimuli. The data were approximated by the Gaussian curve. (c) Spatial frequency characteristics and temporal responses of the detector stimulated by vertical black gratings of various spatial frequencies drifting at the speed of 2.75°/s in the caudo-rostral direction. The spontaneous activity of this cell was very low, of the order of one spike in two seconds, what corresponds to the level which lies well below the horizontal axis. Therefore, it was not marked on the chart. Other conventions are as in Figs. 2 and 3. (d) A polar diagram of the unit measured by dark edges moving in 24 directions against a gray background at the speed of 16.5°/s. The direction of movement of gratings is shown by an open arrow. Other conventions are as in Fig. 1(d).

According to these curves, in the case of linear summation within the RF, the response to high-frequency gratings should be absent, starting from the spatial frequency of about 0.5 cycles per degree. However, the five post-stimulus histograms, shown on the right, demonstrate that it was not the case. To the stimulation by periodic gratings, the cell gave modulated responses, where the width of each burst fit into the period of the grating, which was much narrower than the width of the discharge evoked by the drifting contrast edge.

Just as in the case of the DS GCs, significant changes in stimulation parameters (intensity, contrast and speed of movement of gratings) were shown to have little effect on the spatial frequency characteristics of the OS GCs.

4. Discussion

4.1. *Detection and resolution*

Numerous behavioral experiments with the use of optomotor drums have shown that fish distinguish periodic gratings at all spatial frequencies, which can be resolved by their cone mosaic (Neave, 1984; Schaerer & Neumeyer, 1996; Dobberfuhl *et al.*, 2005; Haug *et al.*, 2010), what was considered as the evidence that the visual system of fish can resolve such gratings. However, in order to follow a moving high-frequency grating in the optomotor drum, the visual system should only be able to detect the grating and determine in which direction it moves. This ability does not require resolving individual stripes of the grating. It is indeed this property that motion detectors investigated in this paper do possess. There are gratings of such a high spatial frequency, that these detectors cannot resolve them, though still can detect. In this respect, the GCs of the fish retina behave in the same way as the human subjects, which "could detect gratings with spatial frequencies much higher than the resolution limit" (Thibos *et al.*, 1987).

Morphological studies show that the goldfish, unlike primates and some fishes (Collin & Pettigrew, 1988; Temple *et al.*, 2010), do not have a fovea with one-to-one connections between cones and GCs (Johns & Easter, 1977). Therefore, retinal acuity was considered to be determined not by the receptor density, but by the GCs, which integrate receptor signals in the areas of their RFs. The results of the previous study (Maximov *et al.*, 2005b) show that even for GCs with their presumably the smallest RFs there is a considerable convergence of cones onto GCs (up to several hundreds of cones per GC), which would worsen resolution. However, these cells responded to movement of gratings of the spatial frequencies, to which they should not, if they were linear integrators. In doing so, they did not respond to the moving grating by modulated firing (did not resolve individual stripes of the grating), but gave a continuous discharge, thus distinguishing a moving grating from a uniformly gray stimulus, to which the detector did not respond. On the one hand, this explains the high acuity exhibited by goldfish in the optomotor drum, but, on the other hand, it raises a new question: what mechanism allows the GCs with broad receptive fields to detect high-frequency gratings.

4.2. *Nonlinear spatial subunits may explain the detection of fine gratings*

The answer to this question is that the implicit assumption of GCs as simple linear integrators is false. In the linear model, the mean spike rate of the response to fine gratings is negligible because neighboring Gaussian components of the opposite signs in the response to the square-wave stimulus cancel each other — see Fig. 11(b)(*2*). To make the device respond to high-frequency gratings, it is necessary to compose the RF of many subunits with significantly smaller zones of signal summation and to insert rectifier circuits, which would not pass negative signals. Figure 8 shows two circuits of the GC RF. Both of them contain linear integrators at two levels. Subunits (S) are assumed to respond to movement of contrast edges in their relatively small RF. Ganglion cells (G) collect signals from many subunits. Circuit (a) does not contain non-linear elements, so at the high-frequency stimulation by the moving gratings, both positive and negative signals from subunits excited by leading and trailing edges of the grating's stripes are relayed to the GC. In circuit (b) rectifiers are inserted at the outputs of subunits of the RF by which the GC collects only positive signals in response to, say, the leading edges of the stripes. As a result, the GC will give a continuous response, while the edges are moving within the RFs of various subunits. By inserting in the circuit half-wave rectifiers of a certain polarity, we will get schemes of the ON or OFF directional-selective units; by inserting a full-wave rectifier, we will get a scheme of the orientation-selective unit.

The concept of spatial subunits was first expressed by Hochstein & Shapley (1976) in connection with a widespread nonlinear pathway with high spatial resolution in the Y-type GCs of the cat retina. Since then, it became clear that the nonlinear RF
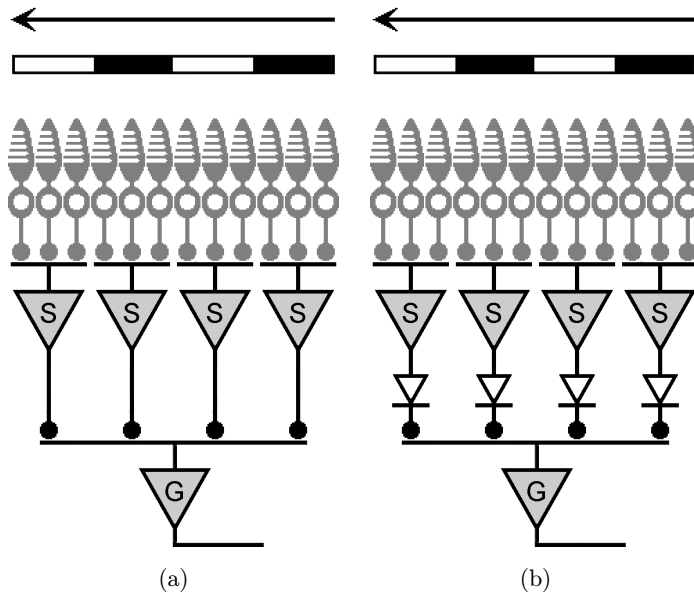

Fig. 8.   Schematic representations of a linear (a) and nonlinear (b) circuits for retinal GCs. Each ganglion cell (G) collects signals from subunits (S), which in turn collect signals from cones.

seems to be expressed by most GC types in all mammalian species (Demb *et al.*, 1999; Schwartz *et al.*, 2012). A morphological substrate of nonlinear subunits in the GC RF was shown to be retinal bipolar cells (Demb *et al.*, 2001). As for the fish retina, such a representation of the nonlinear structure of RFs of detectors of oriented lines has become necessary for explanation of the features of lateral inhibition initiated inside their RRF (Damjanović *et al.*, 2009b). Later on, this and other properties of OS GCs were simulated with a functional computer model containing the nonlinear subunits (Maximov, 2010). Among others, the proposed model was able to detect high-frequency drifting gratings.

4.3. *Computer simulation of the responses of detectors of oriented lines to high-frequency gratings*

A detailed one-dimensional functional model of OS GCs has been described elsewhere (Maximov, 2010). The model reproduced the main physiological properties of these cells, in particular: (1) the absence of responses to homogeneous illumination and presence of sustained responses to edges and stripes of any sign of contrast switched on and off or moving across the RF; (2) a high contrast sensitivity and independence of the magnitude of responses on the brightness (under the conditions of sufficient contrast) when stimulated by flashing stripes or moving edges; (3) the validity of the Weber-Fechner law; (4) the existence of a narrow central excitatory zone that is notably smaller than the RRF, flanked on both sides by inhibitory areas that are extending far beyond the limits of the RRF; (5) the high spatial acuity when tested by moving periodic gratings. To meet the above requirements, in addition to the units specified in the scheme of Fig. 8(b), the model includes two levels of lateral inhibition, as well as the sigmoid nonlinearity in subunits, which ensures high contrast sensitivity and independence of the unit responses on the intensity and contrast.

In this model, the cones arranged in a one-dimensional array were assumed to be separated by a distance of 0.2 angular degrees, according to the measurements by Maximov *et al.* (2005b) in the *C. gibelio* retina. Two parameters of the model, the width of zones of signal summation of subunits and the width of zones of signal summation of GCs, were chosen so as (1) to provide the size of the RF of the order of values shown in the present experiments and (2) to provide its detection acuity in the region of two cycles per degree. To satisfy the requirement of high detection acuity, the width of "receptive field" of subunits was made quite small. Each subunit was connected to three neighboring cones, the input weights of the lateral cones being half that of the central one. On the contrary, the width of "receptive field" of the model GCs was chosen rather large — each GC summed signals of 25 subunits. In this case the value of σ_{RF}, as determined by the response of the model to motion of contrast edge across the RF, was equal $1.38°$, which amounted to 6.9 intercone distances in the model.

Figure 9 shows the responses of the model calculated for different moving stimuli. Upper row (*1*) is the response to a motion of a black edge. The RF size of the model
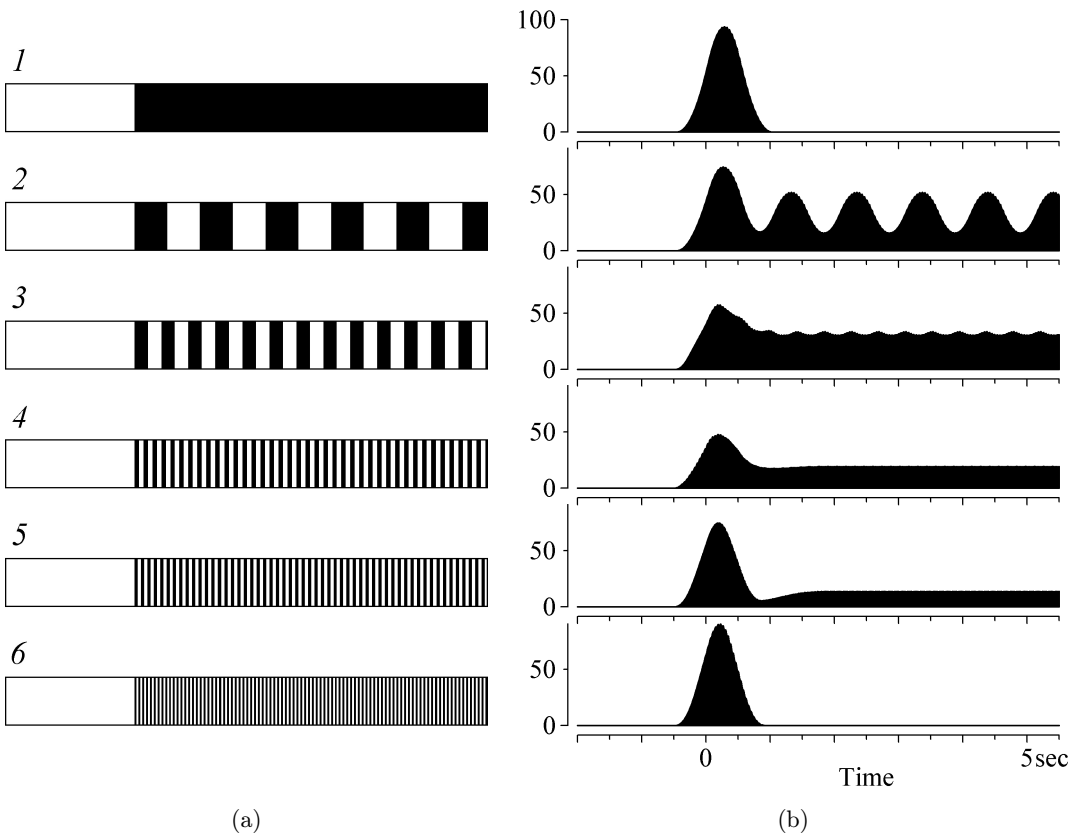
Fig. 9.   Responses of the model of OS GCs to gratings moving across their RF. (a) Stimuli. (b) The time courses of responses of the model GC to movement of a black edge (*1*) and square-wave gratings of various spatial frequencies (*2–6*).

GC was estimated from this reaction by fitting the burst by a Gaussian curve. To the movement of the low-frequency gratings, the model gave more or less modulated responses (rows *2* and *3*). But with increase of the grating frequency, the modulation disappears (the model loses its ability to resolve individual stripes). And to high-frequency gratings close to the limit of detection acuity the model gave unmodulated sustained discharges (rows *4* and *5*). The presence of the sustained responses suggests that the model GC sees the gratings, moving across its RF, but cannot determine their frequencies. Finally, with the further increase of the grating frequency, the sustained response disappears (*6*). Only a burst to the leading edge of the grating remains. At this point, the model achieved the detection threshold and does not distinguish a high-frequency grating from a uniform stimulus. For the chosen parameters of the model, this point corresponds to the grating with stripes lying more densely than cones — the width of the stripes was 0.75 of the intercone distance.

Besides temporal responses shown in Fig. 9, the dependence of the magnitude of the model response on the spatial frequency was calculated for the model. For this, an average response over a period of stimulation was calculated. The period was chosen
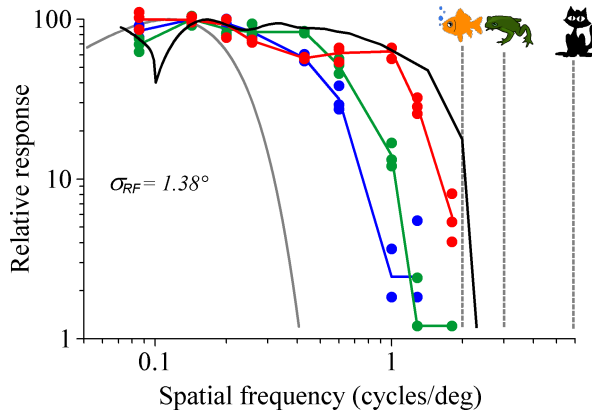
Fig. 10. Spatial frequency dependencies of the mean responses to gratings for three movement detectors of the fish retina (shown in color) and for the computer model of OS GCs (Maximov, 2010) shown by the black curve. Circle marks correspond to spike rates of the units' responses to stimulation with gratings of various spatial frequencies in three separate runs. Other conventions are as in Fig. 3.

sufficiently far from the moment when a leading edge of the grating passes through the RF of the model GC to avoid the effect of transients. The calculated dependence is shown in Fig. 10 by the smooth black curve. Figure 10 shows also three arbitrary experimental curves and the theoretical curve for the linear model. The dashed vertical lines correspond to visual acuity obtained in behavioral experiments for the goldfish and (for comparison) for the frog (Birukow, 1937; Aho, 1997) and the cat (Donaghy, 1980). The detection acuity of the model appeared to be slightly higher than its average values obtained in the present experiments. But it can be easily adjusted by the value of span of areas of signal summation of subunits in the model. As it might be expected, other parameters of the model (in particular, the size of summation area of GCs) have practically no effect on the curve. From this analysis, we can conclude that the detection acuity in the goldfish OS GCs is limited by the width of the RF of subunits.

Despite the fact that the simulation of the direction-selectivity has been extensively developing for a long time (Torre & Poggio, 1978; Grzywacz & Koch, 1987; Borg-Graham & Grzywacz, 1992; Poznanski, 1992, 2005, 2010; Tukker *et al.*, 2004), there is no such model, which would calculate a similar curve for DS GCs.

In addition to the effect, that the experimental curve for the dependence of the mean spike rate of the response (or the magnitude of the zero harmonic component of the Fourier decomposition of the response) on spatial frequency is, as a rule, above the corresponding curve for the first harmonic and above the theoretical curve for the linear model, one more result was obtained in the present study. It was shown, that GCs can resolve individual stripes of the grating at spatial frequencies higher than those predicted by the linear model. That can be seen from comparison of the curves for the first harmonic (which reflects the resolution properties of units), marked with squares in Figs. 3−7, with theoretical curves for the linear model (gray curves). Unfortunately, the mechanisms of this effect remain unexplained.

4.4. *Mosaics of ganglion cells*

Many types of GCs in the retina of vertebrates are packaged in such a way that their dendritic trees densely tile the retinal surface without gaps or overlaps (Wässle *et al.*, 1981; Rockhill *et al.*, 2000; Anishchenko *et al.*, 2010). In particular, the DS GCs of each subtype in the rabbit (Vaney, 1994; Amthor & Oyster, 1995) and mouse (Yonehara *et al.*, 2009) retinas are arranged in this way. There is a reason to assume that in fish each of six subtypes of DS GCs tiles the retina in a similar manner (Maximova *et al.*, 2006). It would seem that the interdependence of the RF size and density of the GCs provides a simple, solely histological method to determine the resolution of the retina, without resorting to either behavioral or electrophysiological studies. In this paper we have tried to show that the resolution is not uniquely defined by sizes of RFs of the retinal GCs or by their density, but also depends on the mode of processing of visual information in the RF. In a completely linear system (Fig. 8(a)) the resolution indeed will be determined by the size of the RF. In the system with rectifiers (Fig. 8(b)), one can obtain the detection of the high-frequency gratings.

In general, the spatial resolution is not determined by the size of the RF of GCs or their density, or the number of fibers in the optic nerve. A webcam has a very large RF and is connected to a computer with a single guide, but provides a very good spatial resolution. The points are, how complex are the messages sent through the fibers of the optic nerve, how complex signal processing is performed in the retina when forming these messages, and how complex is a device that decodes these signals in the brain? All these questions require a physiological approach.

Thus, we can conclude that in the domain of drifting periodic gratings the visual acuity is characterized by two parameters: the acuity of detection (when the grating can be discriminated from a uniform field) and the acuity of resolution (when the animal differentiates individual stripes of the grating). In this paper at the example of motion detectors of the fish retina it was shown that in a nonlinear system the detection limit of periodic gratings can be well above the limit of their resolution, and the visual acuity of a quite complex (nonlinear) system is not determined by the density of its constituent units, because each unit is able to detect high-frequency gratings by itself. Therefore, it is impossible to estimate the visual acuity by the density of the GCs and the size of their RFs.

Appendix: Simple Linear Model of the RF

Let the response of the linear system to an edge, described by a step function

$$h(x) = \begin{cases} 0 & \text{if } x \le 0 \\ 1 & \text{if } x > 0 \end{cases}$$

moving through the RF, will be a Gaussian:

$$g(x) = \frac{N}{\sigma\sqrt{2\pi}} \exp\left(-\frac{x^2}{2\sigma^2}\right),$$

where σ is a standard deviation determining RF width and N is a total number of spikes in the discharge (see Fig. 11(a)).

A square-wave grating with period T can be represented by an infinite sum of steps:

$$s(x) = \sum_{n=-\infty}^{+\infty} (-1)^n h\left(x - \frac{nT}{2}\right). \tag{1}$$

Then the response of the linear system to presentation of the square-wave grating can be calculated as a superposition of the responses of the system to the step functions:

$$r(x) = \sum_{n=-\infty}^{+\infty} (-1)^n g\left(x - \frac{nT}{2}\right).$$

Figure 11(b) illustrates the process of composition of the response of the linear system to the square-wave grating. This yields an even periodic function with a fundamental angular frequency equal to $\frac{2\pi}{T}$, determined by the period of stimulation T (Figs. 11(b)(3)). The spatial resolution of such a linear system can be estimated by the relative magnitude of the first harmonic in the response, which is given by:

$$a = \frac{2}{T} \int_0^T r(x) \cdot \cos\left(\frac{2\pi}{T} x\right) \cdot dx.$$

The corresponding curve calculated for σ equal to 1.4 degrees, is shown in Fig. 11(c). For other values of the σ, the curve has the same form, but shifted along the x-axis.
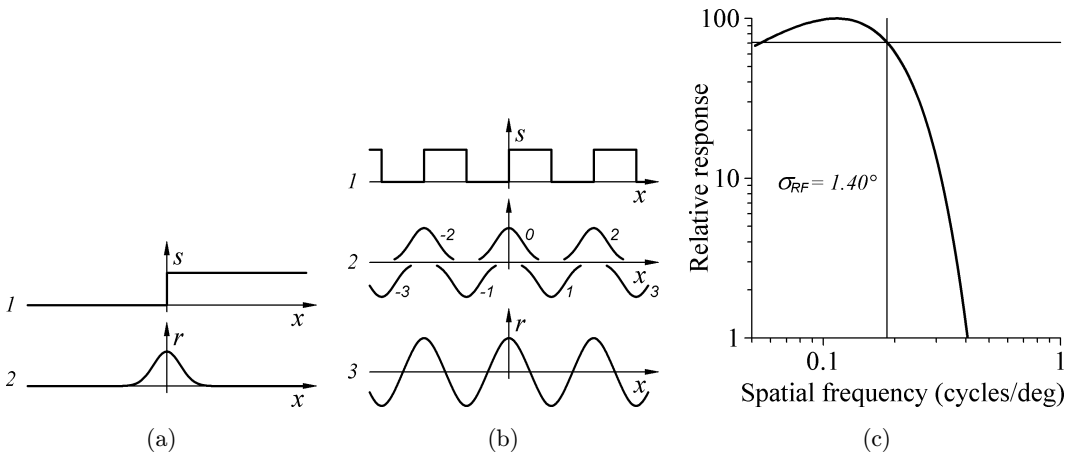

Fig. 11.   Simple linear model of the RF of movement detectors. (a) A stimulus in the form of the Heaviside step function (1) and a Gaussian response of the system (2). (b) A square-wave stimulus (1), responses of the system to different positive and negative steps of the square-wave function (2) and an overall response of the system to the square-wave stimulus (3). The numbers next to the individual Gaussians in (2) correspond to values of n in Eq. (1). (c) The dependence of the amplitude of the first harmonic of the system response elicited by square-wave stimuli on their spatial frequencies. A cross of thin lines marks the cutoff frequency of the system.

One can see that the transfer function of these filters dramatically decreases after a certain frequency. Low-pass filters are commonly characterized by the cutoff frequency where the gain drops to 0.71 of its maximum value. However, for the frequency, which characterizes the spatial resolution in case of GCs, some higher frequency should be used, namely, the highest spatial frequency that produced a reliable response above the endogenous noise of the cell.

Acknowledgments

REFERENCES

Aho, A.-C. (1997) The visual acuity of the frog (*Rana pipiens*). *J. Comp. Physiol. A*, **180**, 19−24.

Amthor, F.R. & Oyster, C.W. (1995) Spatial organization of retinal information about the direction of image motion. *Proc. Natl. Acad. Sci. U.S.A.*, **92**, 4002−4005.

Anishchenko, A., Greschner, M., Elstrott, J., Sher, A., Litke, A.M., Feller, M.B. & Chichilnisky, E.J. (2010) Receptive field mosaics of retinal ganglion cells are established without visual experience. *J. Neurophysiol.*, **103**, 1856−1864.

Bilotta, J. & Powers, M.K. (1991) Spatial contrast sensitivity of goldfish: Mean luminance, temporal frequency and a new psychophysical technique. *Vision Res.*, **31**, 577−585.

Birukow, G. (1937) Untersuchungen über den optischen Drehnystagmus und über die Sehrschärfe des Grasfrosches (*Rana temporaria*). *Z. Vergl. Physiol.*, **25**, 91−142.

Borg-Graham, L.J. & Grzywacz, N.M. (1992) A model of the directional selectivity circuit in retina: Transformations by neurons singly and in concert. In: T. McKenna and J. Davis, eds. *Single Neuron Computation.* NY: Academic Press, pp. 347−376.

Browman, H.I., Gordon, W.C., Evans, B.I. & O'Brien, W.J. 1990. Correlation between histological and behavioral measures of visual acuity in a zooplanktivorous fish, the white crappie (*Pomoxis annularis*). *Brain Behav. Evol.*, **35**, 85−97.

Burrill, J.D. & Easter, S.S. Jr (1994) Development of the retinofugal projections in the embryonic and larval zebrafish (*Brachydanio rerio*). *J. Comp. Neurol.*, **346**, 583−600.

Collin, S.P. & Pettigrew, J.D. (1988) Retinal topography in reef teleosts. I. Some species with well-developed areae but poorly-developed streaks. *Brain Behav. Evol.*, **31**, 269−282.

Cronly-Dillon, J.R. (1964) Units sensitive to direction of movement in goldfish tectum. *Nature*, **203**, 214−215.

Damjanović, I., Maximova, E.M. & Maximov, V.V. (2009a) Receptive field sizes of direction-selective units in the fish tectum. *J. Integr. Neurosci.*, **8**, 77−93.

Damjanović, I., Maximova, E.M. & Maximov, V.V. (2009b) On the organization of receptive fields of orientation-selective units recorded in the fish tectum. *J. Integr. Neurosci.*, **8**, 323−344.

Deguchi, T., Suwa, H., Yoshimoto, M., Kondoh, H. & Yamamoto, N. (2005) Central connection of the optic, oculomotor, trochlear and abducens nerves in medaka, *Oryzias latipes*. *Zoological Science*, **22**, 321−332.

Demb, J.B., Haarsma, L., Freed, M.A. & Sterling, P. (1999) Functional circuitry of the retinal ganglion cell's nonlinear receptive field. *J. Neurosci.*, **19**, 9756−9767.

Demb, J.B., Zaghloul, K., Haarsma, L. & Sterling, P. (2001) Bipolar cells contribute to nonlinear spatial summation in the brisk-transient (Y) ganglion cell in mammalian retina. *J. Neurosci.*, **21**, 7447−7454.

DeVries, S.H. & Baylor, D.A. (1997) Mosaic arrangement of ganglion cell receptive fields in rabbit retina. *J. Neurophysiol.*, **78**, 2048−2060.

Dobberfuhl, A.P., Ullmann, J.F.P. & Shumway, C.A. (2005) Visual acuity, environmental complexity, and social organization in African cichlid fishes. *Behavioral Neuroscience*, **119**, 1648−1655.

Donaghy, M. (1980) The contrast sensitivity, spatial resolution and velocity tuning of the cat's optokinetic reflex. *J. Physiol. (Lond.)*, **300**, 353−365.

Enroth-Cugell, C. & Robson, J.G. (1966) The contrast sensitivity of retinal ganglion cells of the cat. *J. Physiol. (Lond.)*, **187**, 517−552.

Gabriel, J.P., Trivedi, C.A., Maurer, C.M., Ryu, S. & Bollmann1, J.H. (2012) Layer-specific targeting of direction-selective neurons in the zebrafish optic tectum. *Neuron*, **76**, 1147−1160.

Gestesland, R.C., Howland, B., Lettvin, J.Y. & Pitts, W.H. (1959) Comments on micro-electrodes. *Proc IRE*, **47**, 1856−1862.

Grzywacz, N.M. & Koch, C. (1987) Functional properties of models for direction selectivity in the retina. *Synapse*, **1**, 417−434.

Hairston, N.G. Jr, Li, K.T. & Easter, S.S. Jr (1982) Fish vision and the detection of planktonic prey. *Science*, **218**, 1240−1242.

Haug, M.F., Biehlmaier, O., Mueller, K.P. & Neuhauss, S.C.F. (2010) Visual acuity in larval zebrafish: Behavior and histology. *Frontiers in Zoology*, **7**, 8.

Hochstein, S. & Shapley, R.M. (1976) Linear and nonlinear spatial subunits in Y cat retinal ganglion cells. *J. Physiol. (Lond.)*, **262**, 265−284.

Hodos, W. & Yolen, N.M. (1976) Behavioral correlates of "tectal compression" in goldfish. II. Visual acuity. *Brain Behav. Evol.*, **13**, 468−474.

Jacobson, M. & Gaze, R.M. (1964) Types of visual response from single units in the optic tectum and optic nerve of the goldfish. *Qurt. J. Exp. Physiol.* **49**, 199−209.

Johns, P.R. & Easter, S.S. Jr (1977) Growth of the adult goldfish eye. II. Increase in retinal cell number. *J. Comp. Neurol.*, **176**, 331−342.

Lee, S. & Stevens, C.F. (2007) General design principle for scalable neural circuits in a vertebrate retina. *Proc. Nat. Acad. Sci. U.S.A.*, **104**, 12931−12935.

Li, K., Wetterer, T.J. & Hairston, N.G. (1985) Fish size, visual resolution and prey selectivity. *Ecology*, **66**, 1729−1735.

Maximov, V.V. (2010) A model of receptive field of orientation-selective ganglion cells of the fish retina, *Sensory Systems*, **24**, 110−124 (in Russian).

Maximov, V.V., Maximova, E.M. & Maximov, P.V. (2005a) Direction selectivity in the goldfish tectum revisited. *Ann. NY Acad. Sci.*, **1048**, 198−205.

Maximov, V.V., Maximova, E.M. & Maximov, P.V. (2005b) Classification of direction-selective units recorded in the goldfish tectum. *Sensory Systems*, **19**, 322−335 (in Russian).

Maximov, V.V., Maximova, E.M. & Maximov, P.V. (2007) Colour properties of the direction-selective motion detectors projecting to the goldfish tectum. *Sensory Systems*, **21**, 19−28 (in Russian).

Maximov, V.V., Maximova, E.M. & Maximov, P.V. (2009) Classification of orientation-selective units recorded in the goldfish tectum. *Sensory Systems*, **23**, 13−23 (in Russian).

Maximova, E.M. (1999) Colour and spatial properties of detectors of oriented lines in the fish retina. *Iugoslav. Physiol. Pharmacol. Acta.* **34**, 351−358.

Maximova, E.M., Levichkina, E.V. & Utina, I.A. (2006) Morphology of putative direction-selective ganglion cells traced with DiI in the fish retina, *Sensory Systems*, **20**, 279−287 (in Russian).

Maximova, E.M. & Maximov, V.V. (1981) Detectors of the oriented lines in the visual system of the fish *Carassius carassius. J. Evol, Biochem, Physiol.*, **17**, 519−525 (in Russian).

Maximova, E.M., Orlov, O.Yu. & Dimentnman, A.M. (1971) Investigation of visual system of some marine fishes. *Voprocy Ichtiologii*, **11**, 893−899 (in Russian).

Maximova, E.M., Pushchin, I.I., Maximov, P.V. & Maximov, V.V. (2012) Presynaptic and postsynaptic single-unit responses in the goldfish tectum as revealed by a reversible synaptic transmission blocker. *J, Integr. Neurosci.*, **11**, 183−191.

Miller, T.J., Crowder, L.B. & Rice, J.A. (1993) Ontogenetic changes in behavioural and histological measures of visual acuity in three species of fish. *Environ. Biol. Fishes*, **37**, 1−8.

Mora-Ferrer, C., Hausselt, S., Schmidt Hoffmann, R., Ebisch, B., Schick, S., Wollenberg, K., Schneider, C., Teege, P. & Jürgens, K. (2005) Pharmacological properties of motion vision in goldfish measured with the optomotor response. *Brain Res.*, **1058**, 17−29.

Mussi, M., McFarland, W.N. & Domenici, P. (2005) Visual cues eliciting the feeding reaction of a planktivorous fish swimming in a current. *J. Exp. Biol.*, **208**, 831−842.

Nakamura, E.L. (1968) Visual acuity of two tunas, *Katsuwonus pelamis* and *Euthynnus affinis. Copeia*, **1968**, 41−49.

Neave, D.A., (1984) The development of visual acuity in larval plaice (*Pleuronectes platessa* L.) and turbot (*Scophthalmusmaximus* L.). *J. Exp. Mar. Biol. Ecol.*, **78**, 167−175.

Neumeyer C. (2003) Wavelength dependence of visual acuity in goldfish. *J. Comp. Physiol. A*, **189**, 811−821.

Nikolaou, N., Lowe, A.S., Walker, A.S., Abbas, F., Hunter, P.R., Thompson, I.D. & Meyer, M.P. (2012) Parametric functional maps of visual inputs to the tectum. *Neuron*, **76**, 317−324.

Northcutt, R.G. & Wullimann, M.F. (1988) The visual system in teleost fishes. Morphological patterns and trends. In: J. Atema, R.R. Fay, A.N. Popper and W.N. Tavolga, eds. *Sensory Biology of Aquatic Animals*. NY: Springer, pp. 515−552.

Northmore, D.P.M. & Dvorak, C.A. (1979) Contrast sensitivity and acuity of the goldfish. *Vision Res.*, **19**, 255−261.

Northmore, D.P.M., Oh D.-J. & Celenza, M.A. (2007) Acuity and contrast sensitivity of the bluegill sunfish and how they change during optic nerve regeneration. *Vis. Neurosci.*, **24**, 319−331.

Peichl, L. & Wässle, H. (1979) Size, scatter and coverage of ganglion cell receptive field centres in the cat retina. *J. Physiol. (Lond.)*, **291**, 117−141.

Poznanski, R.R. (1992) Modeling the electrotonic structure of starburst amacrine cells in the rabbit retina: A functional interpretation of dendritic morphology. *B. Math. Biol.*, **54**, 905−928.

Poznanski, R.R. (2005) Biophysical mechanism and essential topography of directionally selective subunits in rabbit's retina. *J. Integr. Neurosci.*, **4**, 341−361.

Poznanski, R.R. (2010) Cellular inhibitory behavior underlying the formation of retinal direction selectivity in the starburst network. *J. Integr. Neurosci.*, **9**, 299−336.

Rockhill, R.L., Euler, T. & Masland, R.H. (2000) Spatial order within but not between types of retinal neurons. *Proc. Natl. Acad. Sci. U.S.A.*, **97**, 2303−2307.

Schaerer, S. & Neumeyer, C. (1996) Motion detection in goldfish investigated with the optomotor response is "color blind". *Vision Res.*, **36**, 4025−4034.

Schwartz, G.W., Okawa, H., Dunn, F.A., Morgan, J.L., Kerschensteiner D., Wong, R.O. & Rieke, F. (2012) The spatial structure of a nonlinear receptive field. *Nat. Neurosci.*, **15**, 1572−1580.

Sharma, S.C. (1972) The retinal projections in the goldfish: An experimental study. *Brain Res.* **39**, 213−223.

Temple, S., Hart, N.S., Marshall, N.J. & Collin, S.P. (2010) A spitting image: Specializations in archerfish eyes for vision at the interface between air and water. *Proc. R. Soc. Lond. B*, **277**, 2607−2615.

Thibos, L.N., Cheney, F.E. & Walsh, D.J. (1987) Retinal limits to the detection and resolution of gratings. *J. Opt. Soc. Am. A.*, **4**, 1524−1529.

Torre, V. & Poggio, T. (1978) A synaptic mechanism possibly underlying directional selectivity to motion. *Proc. R. Soc. Lond. B*, **202**, 409−416.

Tukker, J.I., Taylor, R.W. & Smith, R.G. (2004) Direction selectivity in a model of the starburst amacrine cell. *Vis. Neurosci.*, **21**, 611−627.

Vaney, D.I. (1994) Territorial organization of direction-selective ganglion cells in rabbit retina. *J. Neurosci.*, **14**, 6301−6316.

Wässle, H., Peichl, L. & Boycott, B.B. (1981) Dendritic territories of cat retinal ganglion cells. *Nature*, **292**, 344−345.

Yonehara, K., Ishikane, H., Sakuta, H., Shintani, T., Nakamura-Yonehara, K., Kamiji, N.L., Usui, S. & Noda, M. (2009) Identification of retinal ganglion cells and their projections involved in central transmission of information about upward and downward image motion. *PLoS ONE*, **4**, e4320.

Zenkin, G.M. & Pigarev, I.N. (1969) Detector properties of the ganglion cells of the pike retina. *Biophysics*, **14**, 763−772.